

THERMAL STABILITY OF GIANT THERMOPOWER

IN SrTiO₃/SrTi_{0.8}Nb_{0.2}O₃ SUPERLATTICES AT 900 K

Kyu Hyoung Lee, Yoriko Mune ; Hiromichi Ohta, Kunihito Koumoto

Department of Applied Chemistry, Graduate School of Engineering, Nagoya University,
Nagoya 464-8603, Japan

Contact author: koumoto@apchem.nagoya-u.ac.jp

Here we report stability and carrier transport properties of [(SrTiO₃)_x/(SrTi_{0.8}Nb_{0.2}O₃)₁]₂₀ ($x = 0 \sim 50$) superlattices at high temperatures ($T = 300 \sim 900$ K). No significant structural change was observed in the superlattices after annealed at 900 K in vacuum. The Seebeck coefficient of the [(SrTiO₃)₂₀/(SrTi_{0.8}Nb_{0.2}O₃)₁]₂₀ superlattice, which was 300 μVK^{-1} at room temperature, gradually increased with temperature and reached 450 μVK^{-1} at 900 K, which is ~ 3 times larger than that of bulk SrTi_{0.8}Nb_{0.2}O₃, clearly evidenced that the superlattice is stable and exhibits giant Seebeck coefficient even at high temperatures.

Introduction

Recently, we have provided a new class of thermoelectric material: SrTiO₃ having two-dimensional electron gas (2DEG)[1]. The high-density ($\sim 10^{21} \text{ cm}^{-3}$) 2DEG confined within the thickness of a SrTiO₃ unit cell layer ($a = 0.3905 \text{ nm}$), which is realized at SrTiO₃/Nb-doped SrTiO₃ superlattices or TiO₂/SrTiO₃ heterointerfaces. The 2DEG demonstrates that enhanced 2D-thermoelectric Seebeck coefficient ($|S|_{2D}$) by a factor of ~ 5 compared to that for bulk at room temperature. We have also clarified that the origin of the giant $|S|_{2D}$ of SrTiO₃/SrTi_{0.8}Nb_{0.2}O₃ superlattices is quantum size effect [2]: the density of states at the ground state for the SrTi_{0.8}Nb_{0.2}O₃ layer increases inversely proportionally to the insulating SrTiO₃ layer thickness.

If the superlattice structure of SrTiO₃/SrTi_{0.8}Nb_{0.2}O₃ is stable and exhibits

giant $|S|$ even at very high temperature ($T \sim 900$ K), the 2DEG in SrTiO₃/SrTi_{0.8}Nb_{0.2}O₃ superlattices is considered to be a promising candidate for the next generation of thermoelectrics because this system has several advantages, such as good environmental compatibility and high thermal and chemical stability as compared to conventional thermoelectric semiconductors such as Bi₂Te₃ and PbTe [3]. Bulk SrTi_{0.8}Nb_{0.2}O₃ is thermally stable at 1000 K in vacuum or inert gas atmosphere. We have already clarified that the optimized ZT of SrTi_{0.8}Nb_{0.2}O₃ bulk is 0.37 at 1000 K, which is the highest among the reported n -type oxide semiconductor [4]. Thus, clarification of thermal stability and carrier transport properties of SrTiO₃/SrTi_{0.8}Nb_{0.2}O₃ superlattice is critically important for practical thermoelectric application of the 2DEG.

Here we report stability and carrier transport properties of [(SrTiO₃)_x/(SrTi_{0.8}Nb_{0.2}O₃)₁]₂₀ ($x = 0 \sim 50$) superlattices at high temperatures ($T = 300 \sim 900$ K). No significant structural change was observed in the superlattices after annealed at 900 K in vacuum. The $|S|$ of the [(SrTiO₃)₂₀/(SrTi_{0.8}Nb_{0.2}O₃)₁]₂₀ superlattice, which was 300 μVK^{-1} at room temperature, gradually increased with temperature and reached 450 μVK^{-1} at 900 K, which is ~ 3 times larger than that of bulk SrTi_{0.8}Nb_{0.2}O₃, clearly evidenced that the superlattice is stable and exhibits giant $|S|$ even at high temperatures.

Experimental

Superlattices of $[(\text{SrTiO}_3)_x(\text{SrTi}_{0.8}\text{Nb}_{0.2}\text{O}_3)_y]_z$ ($x = 0\sim 50$, $y = 1\sim 20$, $z = 20$) were fabricated on the (001)-face of LaAlO_3 substrates [5] by pulsed laser deposition (PLD, KrF excimer laser, $\lambda = 248$ nm, 20 ns, 10 Hz, $\sim 1 \text{ J}\cdot\text{cm}^{-2}\cdot\text{pulse}^{-1}$) at 950°C in an oxygen atmosphere (oxygen pressure $P_{\text{O}_2} = 1 \times 10^{-3}$ Pa). During film growth of the superlattices, the intensity oscillation of reflection high-energy electron diffraction (RHEED) spots was monitored to control the film deposition precisely. Detail of our film growth method has been described elsewhere [1,2,4]. In order to clarify high temperature stability of the resultant superlattice films, the superlattice was annealed at 900 K in vacuum chamber ($\sim 10^{-3}$ Pa) for several hours. Then, we performed high resolution X-ray diffraction (XRD, ATX-G, Rigaku Co.) measurements of the superlattices to clarify whether intradiffusion of the Nb dopant between the SrTiO_3 layer and $\text{SrTi}_{0.8}\text{Nb}_{0.2}\text{O}_3$ layer occurs or not. Atomic force micrographic (AFM, Nanoscope E, Digital Instruments) observation of the superlattices was also performed.

Results and Discussion

Figure 1 shows the high-resolution XRD patterns and topographic AFM images of the $[(\text{SrTiO}_3)_{20}(\text{SrTi}_{0.8}\text{Nb}_{0.2}\text{O}_3)_1]_{20}$ superlattice. Satellite peaks due to superlattices are clearly observed in the XRD patterns of $[(\text{SrTiO}_3)_{20}(\text{SrTi}_{0.8}\text{Nb}_{0.2}\text{O}_3)_1]_{20}$ around the Bragg peak of 002 SrTiO_3 (0). Atomically flat terraces and steps, which correspond to a unit cell height of SrTiO_3 , are clearly seen in the AFM image, indicating that 2D growth occurred. No significant change is observed in both XRD patterns and AFM images, suggesting that intradiffusion of Nb dopant between SrTiO_3 layer and $\text{SrTi}_{0.8}\text{Nb}_{0.2}\text{O}_3$

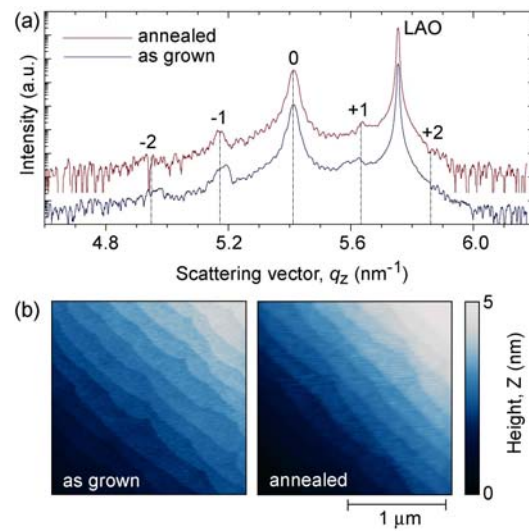


Fig. 1 High-temperature stability of the $[(\text{SrTiO}_3)_{20}(\text{SrTi}_{0.8}\text{Nb}_{0.2}\text{O}_3)_1]_{20}$ superlattice. (a) High-resolution XRD patterns and (b) topographic AFM images of the $[(\text{SrTiO}_3)_{20}(\text{SrTi}_{0.8}\text{Nb}_{0.2}\text{O}_3)_1]_{20}$ superlattice (as grown and annealed at 900 K). layer did not occur even at 900 K. Thus, we judged that reliable carrier transport

properties of the superlattices can be obtained at high temperatures.

Electrical conductivity (σ), Hall mobility (μ_{Hall}) and carrier concentration (n_e) of the $[(\text{SrTiO}_3)_x(\text{SrTi}_{0.8}\text{Nb}_{0.2}\text{O}_3)_1]_{20}$ superlattice were measured at several temperatures ($T = 300 \sim 900$ K) by the d.c. four probe method in the van der Pauw configuration, while the $|S|$ values were measured by a conventional steady state method; introducing a temperature gradient in the in-plane direction. Figure 2 summarizes carrier transport properties of the $[(\text{SrTiO}_3)_x(\text{SrTi}_{0.8}\text{Nb}_{0.2}\text{O}_3)_1]_{20}$ superlattice ($x = 0, 1, 3, 9, 25, 30$, and 36) [(a) σ , (b) μ_{Hall} and n_e , and (c) $|S|$]. The σ values decrease gradually with temperature due to the fact that the conduction electrons are scattered by phonon. Since the SrTiO_3 layer is electrically insulating, the σ values proportionally decrease with x value. The σ values of $\text{SrTi}_{0.8}\text{Nb}_{0.2}\text{O}_3$ layer in the $[(\text{SrTiO}_3)_x(\text{SrTi}_{0.8}\text{Nb}_{0.2}\text{O}_3)_1]_{20}$ superlattice (x

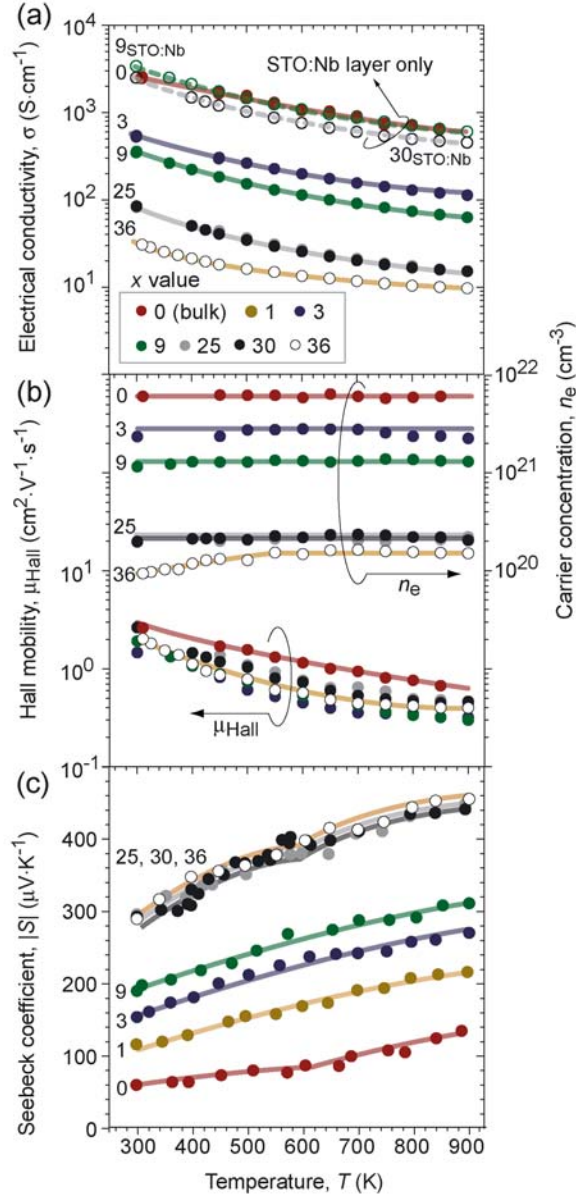


Fig. 2 Carrier transport properties of the $[(\text{SrTiO}_3)_x(\text{SrTi}_{0.8}\text{Nb}_{0.2}\text{O}_3)_1]_{20}$ superlattice ($x = 0, 1, 3, 9, 25, 30,$ and 36) [(a) Electrical conductivity (σ), (b) Hall mobility (μ_{Hall}) and carrier concentration (n_e), and (c) Seebeck coefficient ($|S|$)].

$x = 9$ and 30) are similar to that of $\text{SrTi}_{0.8}\text{Nb}_{0.2}\text{O}_3$ bulk ($x = 0$). No significant temperature dependence of n_e is seen in all cases, while the μ_{Hall} value decreases gradually with temperature indicating that the conduction electrons are scattered by phonons.

On the other hand, the $|S|$ value gradually increases with temperature due to the fact

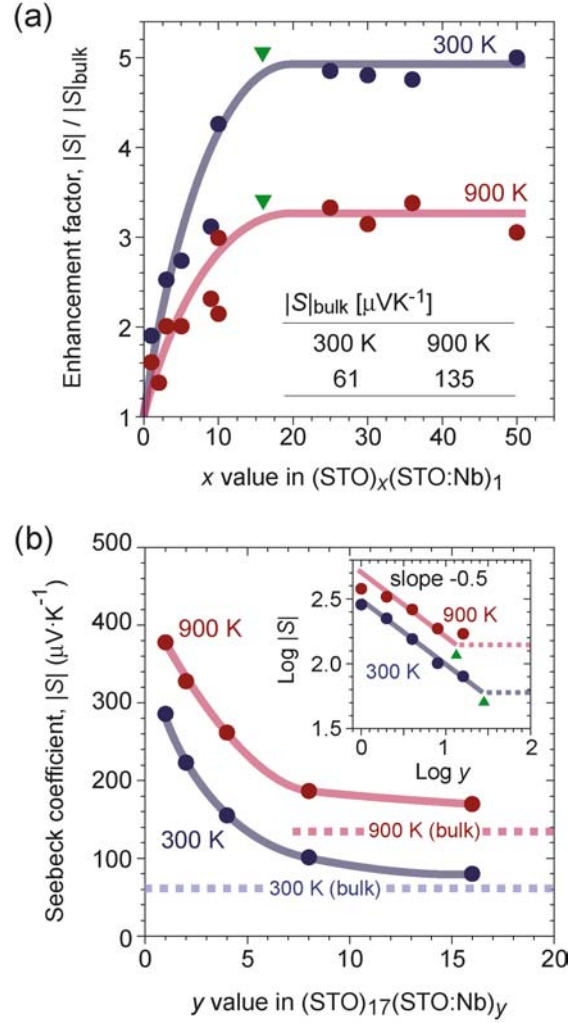


Fig. 3 Seebeck coefficient of the $[(\text{SrTiO}_3)_x(\text{SrTi}_{0.8}\text{Nb}_{0.2}\text{O}_3)_1]_{20}$ superlattices at 900 K. (a) Enhancement factor $|S|/|S|_{\text{bulk}} - x$ plots (red: 900 K and blue: 300 K).

that chemical potential of the material decreases with temperature. The $|S|_{300\text{K}}$ and $|S|_{900\text{K}}$ of $\text{SrTi}_{0.8}\text{Nb}_{0.2}\text{O}_3$ bulk are $61 \mu\text{VK}^{-1}$ and $135 \mu\text{VK}^{-1}$, respectively. It should be noted that the $|S|$ values of the $[(\text{SrTiO}_3)_x(\text{SrTi}_{0.8}\text{Nb}_{0.2}\text{O}_3)_1]_{20}$ superlattices are higher than that of $\text{SrTi}_{0.8}\text{Nb}_{0.2}\text{O}_3$ bulk in the whole temperature range. Figure 3 shows (a) enhancement factor of $|S|$ ($|S|/|S|_{\text{bulk}}$) - x and (b) $|S|$ - y plots for the $[(\text{SrTiO}_3)_x(\text{SrTi}_{0.8}\text{Nb}_{0.2}\text{O}_3)_y]_{20}$ superlattices at 900 K. The $|S|/|S|_{\text{bulk}}$ and $|S|$ values at 300 K are also plotted in the Figs. 3(a) and (b), respectively. The $|S|/|S|_{\text{bulk}}$ value gradually increases with x and saturates when $x > 16$. Although the curve shape at 900 K is similar to the curve at 300 K, the enhancement

factor at 900 K is small ($|S|/|S|_{\text{bulk}} \sim 3$) as compared to that at 300 K ($|S|/|S|_{\text{bulk}} \sim 5$).

On the other hand, a dramatic increase in $|S|_{900\text{K}}$ is seen in Fig. 3(b) with decreasing y -value. When y is 1, $|S|_{900\text{K}}$ reaches $380 \mu\text{V K}^{-1}$, which is ~ 2.8 times larger than that of the $\text{SrTi}_{0.8}\text{Nb}_{0.2}\text{O}_3$ bulk ($|S|_{900\text{K}} = 135 \mu\text{V K}^{-1}$). The slope of the plot of $\log |S|_{2\text{D-}900\text{K}}$ vs. $\log y$ is ~ -0.5 , as shown in the inset, most likely suggesting $\text{DOS}(E) \propto y^{-1.0}$, where E is the ground state energy, which, for the quantum well is given by $E = (\hbar^2 / 2m_d^*) \cdot (\pi / L_z)^2$ [6], where \hbar , m_d^* and L_z are the Planck constant, DOS effective mass and width of the quantum well, respectively. From these results, we concluded that the $[(\text{SrTiO}_3)_x(\text{SrTi}_{0.8}\text{Nb}_{0.2}\text{O}_3)_1]_{20}$ superlattices are stable even at 900 K, and exhibits giant $|S|$ due to the quantum size effect.

It should be noted that the threshold value of y (~ 14 unit cells) for the $|S|$ enhancement at 900 K is smaller than that at 300 K (~ 29 unit cells) as indicated in the inset of Fig. 3(b). Since the thermal de Broglie wavelength ($\lambda_D = \hbar / \sqrt{3 \cdot m^* \cdot k_B \cdot T}$, where \hbar , m^* and k_B are Planck's constant, effective mass of conductive electron, and Boltzmann constant, respectively) of conduction electron decreases proportionally to $T^{-0.5}$, the threshold y value would decrease with temperature. Thus, the enhancement factor of $|S|$ should be small at high temperatures.

In summary, we report stability and carrier transport properties of $[(\text{SrTiO}_3)_x(\text{SrTi}_{0.8}\text{Nb}_{0.2}\text{O}_3)_1]_{20}$ ($x = 0 \sim 50$) superlattices at high temperatures ($T = 300 \sim$

900 K). No significant structural change was observed in the superlattices after annealed at 900 K in vacuum. The $|S|$ of the $[(\text{SrTiO}_3)_{20}/(\text{SrTi}_{0.8}\text{Nb}_{0.2}\text{O}_3)_1]_{20}$ superlattice, which was $300 \mu\text{V K}^{-1}$ at room temperature, gradually increased with temperature and reached $450 \mu\text{V K}^{-1}$ at 900 K, which is ~ 3 times larger than that of bulk $\text{SrTi}_{0.8}\text{Nb}_{0.2}\text{O}_3$, clearly evidenced that the superlattice is stable and exhibits giant $|S|$ even at high temperature.

Based on the present results we have estimated the maximum efficiency of thermoelectric energy conversion for the 2DEG thin layer of Nb-doped SrTiO_3 . Assuming $ZT=2.4$ at 300 K and $ZT=1.9$ at 900 K, the maximum TE conversion efficiency was calculated to be $\sim 22\%$. This is an amazingly high value compared with the case for typical efficiency of bismuth telluride, for instance, which is about 8% under the temperature difference of 200 K. Even though this thin film cannot be applied to power generation for substantial waste heat recovery, this type of nanostructure that could give rise to a quantum confinement effect to generate giant thermopower and reduce the thermal conductivity due to enhanced phonon scattering at nano interfaces simultaneously should be realized in a bulk TE material. SrTiO_3 -related oxide systems would be promising in this sense because of their high phase stability at high temperatures.

References

- [1] H. Ohta, S-W. Kim, Y. Mune, T. Mizoguchi, K. Nomura, S. Ohta, T. Nomura, Y. Nakanishi, M. Hirano, H. Hosono and K. Koumoto, *Nature Mater.* **6**, 129 (2007).
- [2] Y. Mune, H. Ohta, K. Koumoto, T. Mizoguchi and Y. Ikuhara, *Appl. Phys. Lett.* **91**, 192105 (2007).
- [3] J. Wood, *Mater. Today* **10**, 15 (2007).
- [4] S. Ohta, T. Nomura, H. Ohta, M. Hirano, H. Hosono and K. Koumoto, *Appl. Phys. Lett.* **87**, 092108 (2005).
- [5] T. Ohnishi, K. Takahashi, M. Nakagawa, M. Kawasaki, M. Yoshimoto and H. Koinuma, *Appl. Phys. Lett.* **74**, 2531 (1999).
- [6] *Frontiers in Materials Technologies*, ed. by M. A. Meyers and O. T. Inal, Elsevier (Amsterdam – Oxford – New York – Tokyo, 1985).